T-state Inhibitors of *E. coli* Aspartate Transcarbamoylase that Prevent the Allosteric Transition[†,‡]

Sabrina Heng,[§] Kimberly A. Stieglitz,[§] Joby Eldo, Jiarong Xia, James P. Cardia, and Evan R. Kantrowitz*

Department of Chemistry, Merkert Chemistry Center, Boston College, Chestnut Hill, Massachusetts 02467

Received January 18, 2006; Revised Manuscript Received June 21, 2006

ABSTRACT: *Escherichia coli* aspartate transcarbamoylase (ATCase) catalyzes the committed step in pyrimidine nucleotide biosynthesis, the reaction between carbamoyl phosphate (CP) and L-aspartate to form *N*-carbamoyl-L-aspartate and inorganic phosphate. The enzyme exhibits homotropic cooperativity and is allosterically regulated. Upon binding L-aspartate in the presence of a saturating concentration of CP, the enzyme is converted from the low-activity low-affinity T state to the high-activity high-affinity R state. The potent inhibitor *N*-phosphonacetyl-L-aspartate (PALA), which combines the binding features of Asp and CP into one molecule, has been shown to induce the allosteric transition to the R state. In the presence of only CP, the enzyme is the T structure with the active site primed for the binding of aspartate. In a structure of the enzyme−CP complex (T_{CP}), two CP molecules were observed in the active site approximately 7Å apart, one with high occupancy and one with low occupancy. The high occupancy site corresponds to the position for CP observed in the structure of the enzyme with CP and the aspartate analogue succinate bound. The position of the second CP is in a unique site and does not overlap with the aspartate binding site. As a means to generate a new class of inhibitors for ATCase, the domain-open T state of the enzyme was targeted. We designed, synthesized, and characterized three inhibitors that were composed of two phosphonacetamide groups linked together. These two phosphonacetamide groups mimic the positions of the two CP molecules in the T_{CP} structure. X-ray crystal structures of ATCase−inhibitor complexes revealed that each of these inhibitors bind to the T state of the enzyme and occupy the active site area. As opposed to the binding of Asp in the presence of CP or PALA, these inhibitors are unable to initiate the global T to R conformational change. Although the best of these T-state inhibitors only has a K_i value in the micromolar range, the structural information with respect to their mode of binding provides important information for the design of second generation inhibitors that will have even higher affinity for the active site of the T state of the enzyme.

Escherichia coli aspartate transcarbamoylase (E.C. 2.1.3.2, ATCase[1]) catalyzes the committed step in pyrimidine nucleotide biosynthesis, the reaction between carbamoyl phosphate (CP) and L-aspartate, to form *N*-carbamoyl-L-aspartate and inorganic phosphate. The reaction is ordered with CP binding before L-aspartate and *N*-carbamoyl-L-aspartate leaving before inorganic phosphate (*1*). *E. coli* ATCase exhibits cooperativity with respect to the second substrate aspartate (*2*) and exerts allosteric control over the rate of pyrimidine nucleotide metabolism. The enzyme is allosterically inhibited by the end products of the pathway, CTP (*3*) and UTP in the presence of CTP (*4*), and allosterically activated by ATP (*3*), the product of the parallel purine nucleotide biosynthesis pathway. The homotropic and heterotropic properties of the enzyme are manifest by the ability of the enzyme to switch between a low-activity low-affinity T state and a high-activity high-affinity R state.

E. coli ATCase is composed of 12 polypeptide chains. The six larger chains (M_r 34 000) are grouped into two trimers, and the six smaller chains (M_r 17 000) are grouped into three dimers. The active sites are located on the larger or catalytic chains, whereas the allosteric binding sites are located on the smaller or regulatory chains. The catalytic trimers and

[†] This work was supported by Grant GM26237 from the National Institutes of Health.

[‡] X-ray coordinates for the three enzyme−inhibitor complexes have been deposited in the Protein Data Bank as entries 2FZG, 2FZC, and 2FZK.

* To whom correspondence should be addressed. Tel: 617-552-4558. Fax: 617-552-2705. E-mail: evan.kantrowitz@bc.edu.

[§] These authors contributed equally to this work.

[1] Abbreviations: ATCase, *E. coli* aspartate transcarbamoylase holoenzyme; CP, carbamoyl phosphate; PALA, *N*-phosphonacetyl-L-aspartate; PAM phosphonacetamide; C1/C6, the two catalytic chains of ATCase in the asymmetric unit of the crystal; R1/R6, the two regulatory chains of ATCase in the asymmetric unit of the crystal; ASP domain, the portion of the catalytic chain of ATCase primarily involved in binding L-aspartate; CP domain, the portion of the catalytic chain of ATCase primarily involved in binding carbamoyl phosphate; T_{apo}, the X-ray structure of ATCase in the presence of CTP (pdb code: 1ZA1); T_{CP}, the T-state X-ray structure of the aspartate transcarbamoylase holoenzyme in the presence of CTP and CP (pdb code: 1ZA2); T_{PAM}, the X-ray structure of ATCase in the presence of PAM (pdb code: 3AT1); R_{PM} the X-ray structure of ATCase in the presence of PAM and malonate (pdb code: 7AT1); R_{PALA}, the X-ray structure of ATCase in the presence of PALA (pdb code: 1D09); R_{236_PAM}, the X-ray structure of D236A mutant ATCase in the presence of PAM (pdb code: 2A0F); T_1, the T-state X-ray structure of the ATCase holoenzyme in the presence of CTP and 2,2′-(ethane-1,2-diylbis(azanediyl))bis(2-oxoethane-2,1-diyl)diphosphonic acid (**1**); T_2, the T-state X-ray structure of the ATCase holoenzyme in the presence of CTP and 2,2′-(1,3-phenylenebis(azanediyl))bis(2-oxoethane-2,1-diyl)diphosphonic acid (**2**); T_3, the T-state X-ray structure of the ATCase holoenzyme in the presence of CTP and 3,5-bis(2-phosphonoacetamido)benzoic acid (**3**).

10.1021/bi0601095 CCC: $33.50
Published on Web 08/01/2006

regulatory dimers are stable, independent of each other. After separation, the catalytic trimers and regulatory dimers still retain catalytic activity and ability to bind the regulatory nucleotides, respectively. However, homotropic cooperativity is abolished.

In mammalian cells, the first three steps in de novo pyrimidine nucleotide biosynthesis are catalyzed by CAD, a multienzyme complex composed of carbamoyl phosphate synthetase, ATCase and dihydroorotase (*5*). A sequence alignment of the catalytic chain of *E. coli* ATCase with the corresponding portion of CAD reveals that all of the amino acids involved in substrate binding and catalysis are fully conserved (*6*). No structural data is available for the CAD complex; however, the structure of *E. coli* ATCase has been determined in the T and R states in the presence and absence of substrates, substrate analogues, and nucleotide effectors (*7*−*10*).

For the *E. coli* enzyme, the binding of Asp to the enzyme−CP complex causes the two domains of the catalytic chain to close (*10*), which accelerates the reaction by approximation. This mechanism holds for both the holoenzyme as well as the isolated catalytic subunit and is hypothesized to occur in the ATCase portion of CAD as well.

One of the best inhibitors of ATCase is *N*-phosphonacetyl-L-aspartate (PALA) (K_i 27 nM) (*11*). Biochemical and structural studies have shown that the addition of PALA induces the allosteric transition of the enzyme from the T to the R structure (*8*, *12*, *13*). The tight binding of PALA is most likely due to its resemblance to the tetrahedral intermediate in the reaction. Using the X-ray structure of the enzyme−PALA complex, it has been possible to replace PALA with the structure of the tetrahedral intermediate with little or no alterations to the positions of side chains in the active site (*8*). PALA has also been shown to be a good inhibitor of CAD in vitro (*14*, *15*) and has been shown to stop the proliferation of cancer cells in culture (*16*).

Although the structure of the *E. coli* ATCase−PALA complex (R_{PALA}) is in the R-structural state, and the X-ray structure of the *E. coli* ATCase−CP complex (T_{CP}) is in the T-structural state (*10*). In this structure, two molecules of CP are bound in each active site, one with full occupancy and the other with significantly lower occupancy. The high occupancy site corresponds to the position for CP observed in the structure of the enzyme with CP and the aspartate analogue succinate bound (*17*). The position of the second CP is a unique site and does not overlap the aspartate binding site (Figure 1). Because PALA contains in a single molecule the binding features of both aspartate and CP and is similar in structure to the tetrahedral intermediate of the reaction, PALA binds tightly to the domain-closed R state. As a means to generate a new class of inhibitors of aspartate transcarbamoylase targeted at the domain-open T state of the enzyme, we designed, synthesized, and characterized a series of compounds that were composed of two phosphonacetamide groups linked together. The two phosphonacetamide groups mimic the positions of the two CP molecules in the T_{CP} structure. Our goal was to design inhibitors that would bind to the T state and, thereby, prevent the conversion of the enzyme to the R state, trapping the enzyme in the low-activity low-affinity T state.

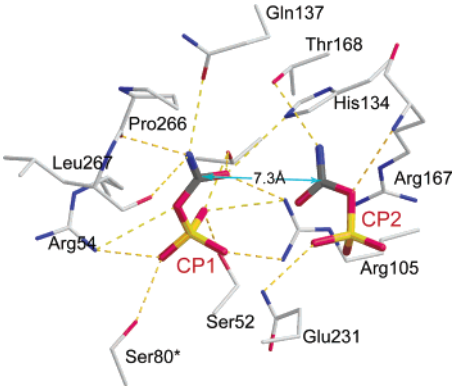

FIGURE 1: Active site of *E. coli* ATCase with CP bound. Two molecules of CP are observed bound to each active site, one with high affinity (CP1) and the other with low affinity (CP2). This distance between the carbonyl carbons of these two molecules is 7.3 Å. This Figure was drawn with POVScript+ (*42*) using pdb entry 1ZA2.

MATERIALS AND METHODS

Materials

Chemicals. CTP, L-aspartate, potassium dihydrogen phosphate, and sodium dodecyl sulfate were obtained from Sigma Chemical Co. (St. Louis, Missouri). Carbamoyl phosphate dilithium salt, obtained from Sigma, was purified before use by precipitation from 50% (v/v) ethanol and was stored desiccated at −20 °C (*18*). The 2-mercaptoethanol and the chemicals used in preparation of the inhibitors were purchased from Aldrich (St. Louis, Missouri).

*Synthesis and Characterization of 2,2′-(Ethane-1,2-diylbis(azanediyl))-bis(2-oxoethane-2,1-diyl)diphosphonic acid (**1**)*

*N,N′-(Ethane-1,2-diyl)bis(2-chloroacetamide) (**1b**)*. Ethane-1,2-diamine (**1a**) (500 mg, 8.3 mmol) was dissolved in anhydrous CH_2Cl_2 (8 mL), and the solution was cooled to 0 °C. Pyridine (3.4 mL, 42 mmol) was dropwise added to **1a** and stirred at 0 °C for 5 min. Chloroacetic anhydride (6 g, 42 mmol) was dissolved in anhydrous CH_2Cl_2 (10 mL), and the solution was added to the reaction mixture via a double-edged needle, under anhydrous conditions. The mixture was allowed to warm up to room temperature and stirred for 18 h. The dark brown precipitate that formed in the reaction vessel after 18 h was collected under vacuum filtration and washed with excess CH_2Cl_2 and H_2O to yield **1b** (957 mg, 54.3%, white, powdery solid). ^{1}H NMR ($(CD_3)_2SO$, 400 MHz) δ 8.28 (br. s 2H), 4.05 (s, 4H), 3.17 (d, J = 2.8 Hz, 4H); ^{13}C NMR ($(CD_3)_2SO$, 400 MHz) δ 165.85, 42.60, 38.80. ESI-MS (m/z) 236.9 $[M + Na]^+$.

*Tetraethyl 2,2′-(ethane-1,2-diylbis(azanediyl))bis(2-oxoethane-2,1-diyl)diphosphonate (**1c**)*. Excess triethyl phosphite (11 mL) was added to **1b** (700 mg, 3.28 mmol), and the reaction was refluxed at 140 °C for 6 h. A white precipitate formed upon the cooling of the reaction mixture to room temperature. Excess triethyl phosphite was decanted, and the precipitate was washed with excess hexane to remove all traces of triethyl phosphite to yield **1c** (950 mg, 69%, fine, white solid). ^{1}H NMR ($(CD_3)_2SO$, 400 MHz) δ 7.75 (br. s 2H), 4.17 (q, J = 6.8 Hz, 8H), 3.36 (d, J = 5.6 Hz, 4H), 2.88 (d, J = 21.2 Hz, 4H), 1.36 (t, J = 7.1 Hz, 12H); ^{13}C

NMR ($(CD_3)_2SO$, 400 MHz) δ 165.47, 63.08, 36.81, 35.50, 17.72; ^{31}P NMR ($(CD_3)_2SO$, 300 MHz) δ 23.62. ESI-MS (*m*/*z*) 417.0 $[M + H]^+$.

*2,2′-(Ethane-1,2-diylbis(azanediyl))bis(2-oxoethane-2,1-diyl)diphosphonic Acid (**1**)*. **1c** (700 mg, 1.6 mmol) was dissolved in CH_3CN (5 mL) and the solution was cooled to 0 °C. Bromotrimethylsilane (1.4 mL, 10.4 mmol) was then added dropwise. The mixture was allowed to warm up to room temperature and stirred for 18 h. Excess solvent was removed under vacuum, resulting in a viscous liquid to which H_2O (3 mL) was added, and the reaction was allowed to stir at room temperature for 1 h. The mixture was washed with CH_2Cl_2 (3 × 10 mL), and the aqueous layer was collected and lyophilized to yield **1** (400 mg, 82%, white solid). ^1H NMR (D_2O, 400 MHz) δ 4.80 (s, 2H), 3.33 (s, 4H), 2.84 (d, J = 21.2 Hz, 4H); ^{31}P NMR (D_2O, 300 MHz) δ 18.458. ESI-MS (*m*/*z*) 304.9 $[M + H]^+$.

*Synthesis and Characterization of 2,2′-(1,3-Phenylenebis-(azanediyl))bis(2-oxoethane-2,1-diyl)diphosphonic Acid (**2**)*

*N,N′-(1,3-Phenylene)bis(2-chloroacetamide) (**2b**)*. Benzene-1,3-diamine (**2a**) (1.5 g, 8.2 mmol) was dissolved in anhydrous DMF (10 mL), and the solution was cooled to 0 °C. Pyridine (3.3 mL, 41 mmol) was added dropwise to **2a** and stirred at 0 °C for 5 min. Chloroacetic anhydride (5.8 g, 41 mmol) was dissolved in anhydrous DMF (10 mL), and the solution was added to the reaction mixture via a double-edged needle, under anhydrous conditions. The mixture was allowed to warm up to room temperature and was stirred for 18 h. CH_2Cl_2 was added to the reaction mixture and a bright yellow precipitate formed. The precipitate was collected under vacuum filtration and was washed with an excess CH_2Cl_2 to yield **2b.** (1g, 46.7%, white, powdery solid). ^1H NMR ($(CD_3)_2SO$, 400 MHz) δ 10.36 (s, 2H), 7.95 (s, 1H), 7.34−7.28 (m, 3H), 4.25 (s, 4H); ^{13}C NMR ($(CD_3)_2SO$, 400 MHz) δ 164.39, 138.64, 129.02, 114.66, 110.18, 43.59. ESI-MS (*m*/*z*) 282.9 $[M + Na]^+$.

*Tetraethyl 2,2′-(1,3-Phenylenebis(azanediyl))bis(2-oxoethane-2,1-diyl)diphosphonate (**2c**)*. Excess triethyl phosphite (10 mL) was added to **2b** (1 g, 3.8 mmol), and the reaction was refluxed at 140 °C for 6 h. Excess triethyl phosphite was removed under reduced pressure to give a yellow, viscous residue, which was further purified by column chromatography using a solvent mixture of CH_3OH/ethyl acetate (1:9) to yield **3c** (1 g, 56%, white solid). ^1H NMR ($(CD_3)_2SO$, 400 MHz) δ 10.15 (s, 2H), 7.88 (s, 1H), 7.25−7.20 (m, 3H), 4.06 (q, J = 6.8, 8H), 3.08 (d, J = 21.6, 4H), 1.24 (t, J = 7.2, 12H); ^{13}C NMR ($(CD_3)_2SO$, 400 MHz) δ 162.66, 139.00, 128.83, 113.96, 109.58, 61.71, 36.51, 35.21, 16.25; ^{31}P NMR ($(CD_3)_2SO$, 300 MHz) δ 22.58. ESI-MS (*m*/*z*) 487.2 $[M + Na]^+$.

*2,2′-(1,3-Phenylenebis(azanediyl))bis(2-oxoethane-2,1-diyl)diphosphonic Acid (**2**)*. **2c** (600 mg, 1.283 mmol) was dissolved in CH_3CN (6 mL), and the solution was cooled to 0 °C. Bromotrimethylsilane (1.08 mL, 8.3 mmol) was then added dropwise. The mixture was allowed to warm up to room temperature and stirred for 18 h. Excess solvent was removed under vacuum, resulting in a viscous liquid to which H_2O (3 mL) was added, and the reaction was allowed to stir at room temperature for 1 h. The mixture was washed with CH_2Cl_2 (3 × 20 mL), and the aqueous layer was collected and lyophilized to yield **2** (453 mg, 99%, light brown solid). ^1H NMR (D_2O, 300 MHz) δ 7.59 (s, 1H), 7.41−7.35 (m, 1H), 7.27−7.24 (m, 2H), 2.98 (d, J = 21, 4H); ^{31}P NMR (D_2O, 300 MHz) δ 23.24. ESI-MS (*m*/*z*) 375.0 $[M + Na]^+$.

*Synthesis and Characterization of 3,5-Bis(2-phosphonoacetamido)benzoic Acid (**3**)*

*3,5-Bis(2-chloroacetamido)benzoic Acid (**3b**)*. 3,5-Diaminobenzoic acid (**3a**) (2 g, 13 mmol) was dissolved in anhydrous DMF (10 mL), and the solution was cooled to 0 °C. Pyridine (5.2 mL, 65 mmol) was added dropwise to **3a** and stirred at 0 °C for 5 min. Chloroacetic anhydride (8.9 g, 65 mmol) was dissolved in anhydrous DMF (10 mL), and the solution was added to the reaction mixture via a double-edged needle, under anhydrous conditions. The mixture was allowed to warm up to room temperature and stirred for 18 h. CH_2Cl_2 was added to the reaction mixture and a bright yellow precipitate formed. The precipitate was collected under vacuum filtration and washed with excess CH_2Cl_2 to yield **3b** (900 mg, 37%, yellow, powdery solid). ^1H NMR ($(CD_3)_2SO$, 400 MHz) δ 10.55 (s, 2H), 8.188 (s, 1H), 7.95 (s, 2H), 4.27 (s, 4H); ^{13}C NMR ($(CD_3)_2SO$, 400 MHz) δ 166.44, 164.65, 138.85, 131.61, 115.28, 43.54.

*3,5-Bis(2-(diethoxyphosphoryl)acetamido)benzoic Acid (**3c**)*. Excess triethyl phosphite (10 mL) was added to **3b** (900 mg, 4.3 mmol), and the reaction was refluxed at 140 °C for 6 h. Excess triethyl phosphite was removed under reduced pressure to give a yellow, viscous residue, which was further purified by column chromatography using a solvent mixture of CH_3OH/ethyl acetate (3:7) to yield **3c** (1.7 g, 78%, white, flaky solid). ^1H NMR ($(CD_3)_2SO$, 300 MHz) δ 10.88 (s, 2H), 8.10 (s, 1H), 7.92 (s, 2H), 4.07 (q, J = 7.4 Hz, 8H), 3.10 (d, J = 21.6 Hz, 4H), 1.25 (t, J = 7.1 Hz, 12H); ^{13}C NMR ($(CD_3)_2SO$, 400 MHz) δ 165.00, 163.07, 139.33, 130.54, 114.37, 61.80, 36.57, 35.28, 16.24, 14.23; ^{31}P NMR ($(CD_3)_2SO$, 300 MHz) δ 22.91.

*3,5-Bis(2-phosphonoacetamido)benzoic Acid (**3**)*. **3c** (200 mg, 0.39 mmol) was dissolved in CH_3CN (4 mL), and the solution was cooled to 0 °C. Bromotrimethylsilane (0.33 mL, 2.5 mmol) was then added dropwise. The mixture was allowed to warm up to room temperature and stirred for 18 h. Excess solvent was removed under vacuum, resulting in a viscous liquid to which H_2O (3 mL) was added, and the reaction was allowed to stir at room temperature for 1h. The mixture was extracted with CH_2Cl_2 (3 × 10 mL), and the aqueous layer was collected and lyophilized to yield **3** (100 mg, 65%, light brown solid). ^1H NMR (D_2O, 400 MHz) δ 10.39 (s, 2H), 8.19 (s, 1H), 7.92 (s, 2H), 3.00 (d, J = 20.8 Hz, 4H); ^{31}P NMR (D_2O, 300 MHz) δ 23.24.

Methods

NMR. ^1H, ^{13}C, and ^{31}P NMR spectra were recorded on Varian Gemini 2000 (400 and 300 MHz) spectrometers. ^1H chemical shifts (δ) are reported in ppm downfield of an internal standard of tetramethylsilane (TMS, δ 0.00) or with the solvent references relative to TMS employed as the internal standard (DMSO-d_6, δ 2.50; D2O, δ 4.79). ^{13}C and ^{31}P chemical shifts are reported with DMSO-d_6 and 85% H_3PO_4, respectively, as references. ESI mass spectrometry was performed at the Mass Spectrometry Facility, Boston College.

Enzyme Preparation. E. coli ATCase holoenzyme and catalytic subunit were overexpressed utilizing *E. coli* strain EK1104 (F^- *ara*, *thi*, Δ(*pro-lac*), Δ*pyrB*, *pyrF*$^{\pm}$, rpsL) (*19*) containing plasmids pEK152 (*20*) and pEK17 (*19*). The isolation and purification were performed as described previously (*19*). The concentration of the holoenzyme and catalytic subunit was determined by A_{280} based upon extinction coefficients of 0.59 and 0.72 cm^2 mg^{-1}, respectively (*21*). The purity of the enzymes was checked by SDS−PAGE (*22*) and nondenaturing PAGE (*23*, *24*).

Crystallization and Freezing of Crystals. ATCase holoenzyme was crystallized by microdialysis, using 50 μL wells. The enzyme solution, at ∼18 mg/mL, was dialyzed against a solution of 40 mM citric acid, 3 mM sodium azide, 1 mM 2-mercaptoethanol, 1 mM cytidine 5′-triphosphate, and 0.2 mM EDTA (pH 5.7) as previously described (*25*). The crystals grew to average dimensions of 0.5 × 0.5 × 0.1 mm within 2 weeks. For structure determination in the presence of inhibitors, enzyme crystals in a microdialysis chamber were dialyzed over 12 h against a crystallization buffer containing 5 mM inhibitor. Crystals were then transferred into a freezing solution containing 30% 2-methyl-2,4-pentanediol in crystallization buffer with 5 mM inhibitor for approximately one minute prior to freezing in liquid nitrogen.

X-ray Data Collection and Processing. The data for the structure for the three enzyme−inhibitor structures were collected using a Rigaku/MSC R-axis IV++ detector, whereas X-rays were generated using a Rigaku/MSC RU-200 rotating-anode generator operating at 50 kV and 100 mA at the Crystallographic Facility in the Chemistry Department of Boston College. The diffraction data were integrated, scaled, and averaged using d*TREK (*26*).

Structural Refinement. The initial model for the T_1, T_2 and T_3 structures was derived from the coordinates of the T_{apo} and T_{CP} structure. Prior to refinement, all of the waters and ligands were removed. The refinement was carried out using CNS (*27*). After initial rigid body, simulated annealing, minimization, and B-factor refinement, initial maps were inspected. The 80's loop of the catalytic chain was disordered, and through several rounds of manual rebuilding, the catalytic chain was corrected using XtalView (*28*). Several cycles of corrections were made to the regulatory chains by repeatedly overlaying the previously published T-state structure, T_{apo}. After rebuilding the 80's loop and 240's loop of the catalytic chains, the inhibitors were fit into the difference density in the active site. Once manual rebuilding was complete, the placement of inhibitors was checked by simulated annealing omit maps calculated in CNS (*27*).

Waters were added to the structure using CNS and XtalView on the basis of F_o-F_c electron density maps at or above the 2.5 σ level and were checked and retained only when they could be justified by hydrogen bonds. The model was checked for errors using PROCHECK (*29*). The details of data processing and refinement statistics are given in Table 1.

Automated Docking Procedure. The program AUTODOCK (*30*) was used for the automated docking of inhibitors to the active site. AUTODOCK was used both in the design of the inhibitors and as an aid in the placement of the inhibitors in the difference density of the final models. To have one complete active site, two adjacent catalytic chains were used for the docking procedure. The grid box was set at 30 $Å^3$ centered at the middle of the active site, with a grid spacing of 0.275 Å between grid points. In each case, 50 docking runs were performed using the Genetic Algorithm with a maximum of 500 000 energy evaluations.

Table 1: Data Collection and Refinement Statistics for the T_1, T_2, and T_3 Structures[a]

data collection	**1**	**2**	**3**
space group	*P*321	*P*321	*P*321
cell dimensions			
$a = b$, c (Å)	120.59, 141.71	119.94, 141.97	120.90, 141.61
α, β, γ (°)	90, 90, 120	90, 90, 120	90, 90, 120
resolution (Å)	27.35−2.00	28.23−2.00	28.45−2.50
R_{merge}[b] (%)	.058 (0.362)	.097 (0.390)	.075 (0.370)
average (I/σ)	13.5 (4.3)	9.7 (3.9)	13.0 (3.9)
completeness (%)	99.9 (99.5)	99.8 (99.6)	99.1 (100)
total reflections	428691	369064	206097
unique reflections	80677	79872	80627
redundancy	5.31 (5.13)	4.62 (4.24)	4.96 (4.78)
refinement			
resolution (Å)	27.35−2.10	28.23−2.25	28.45−2.50
reflections	80493	65470	80627
R_{factor}/R_{free}	.190/0.255	.207/0.249	.210/0.240
RMS deviations			
bonds (Å)	0.008	0.011	0.010
angles (°)	1.57	1.90	1.54
mean *B* value ($Å^2$)	40.8	45.9	42.3
total number of waters	790	252	391

[a] The values in parentheses are for the highest resolution shell.
[b] $R_{merge} = \frac{\sum|I_{hkl} - \overline{I_{hkl}}|}{\sum \overline{I_{hkl}}}$

Fluorescence Measurements. To determine if inhibitors **1**, **2**, and **3** were able to convert the enzyme from the T to the R state in solution, fluorescence spectroscopy was employed in conjunction with a pyrene-labeled version of ATCase that is sensitive to the quaternary structure of the enzyme (*31*). Fluorescence emission spectra were recorded at 20 ± 1 °C in 50 mM Tris-acetate buffer at pH 8.3 on a Shimadzu 1000 spectrofluorimeter. The excitation wavelength was 338 nm, the emission wavelength collected was 350−600 nm, and the excitation and emission bandwidths were set to 5 nm.

RESULTS

Design and Modeling of Inhibitors. In the T_{CP} structure of ATCase, two molecules of CP are observed in the active site, one with full occupancy and the other with significantly lower occupancy (Figure 1). The position of these two CP molecules in the T-state active site suggested that a new class of T-state inhibitors of ATCase might be designed by linking two phosphonacetamide units together. In the T_{CP} structure, the carbonyl carbons of CP are 7.3 Å apart (Figure 1). On the basis of this separation distance, a number of inhibitor candidates were designed. AUTODOCK was used to provide possible orientations of these inhibitors in the active site and to calculate their relative affinities for the enzyme. Scrutiny of the AUTODOCK results for **1** bound in the active site revealed that if the aliphatic functionality that linked the two phosphonacetamide moieties was replaced with an aromatic ring, the resulting compound would not only be able to

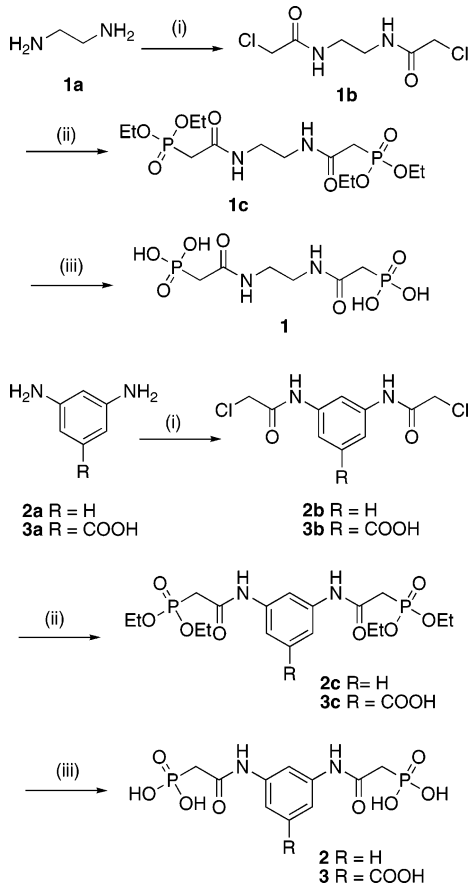

FIGURE 2: Synthetic scheme for inhibitors **1**, **2**, and **3**. (i) $(ClCH_2CO)_2O$, pyridine, THF, 0 °C−r.t., 18 h; (ii) $P(OEt)_3$, 140 °C, 6 h; (iii) TMSBr, CH_3CN, 0 °C−r.t., 18 h, then H_2O, r.t., 1 h.

increase the hydrophobic interactions with the 260's loop but also be able to improve the distance between the two carbonyls closer to the target distance of 7.3 Å. True to our hypothesis, AUTODOCK results indicated that **2** and **3** had better binding energies than PALA in the T state. On the basis of these AUTODOCK results, inhibitor candidates **1**, **2**, and **3** were synthesized (Figure 2).

Inhibitor Synthesis. **1a**, **2a**, and **3a** (Figure 2) were acylated with chloroacetic anhydride in the presence of pyridine (*32*−*34*) to give **1b**, **2b**, and **3b**, respectively. Refluxing the acylated products at 140 °C in triethyl phosphite (*35*) yielded **1c**, **2c**, and **3c**, respectively. Final compounds **1**, **2**, and **3** were deprotected using bromotrimethylsilane in a single pot at 0 °C (*36*).

Inhibition Studies. Because of homotropic cooperativity and strong substrate inhibition, only IC_{50} values could be determined for the ATCase holoenzyme. At pH 8.3 in 0.1 M Tris-acetate buffer, the IC_{50} values for **1**, **2**, and **3** were 200, 86, and 79 μM, respectively. A more detailed kinetic characterization of the inhibitors was performed on the catalytic subunit with respect to both substrates, Asp and CP. Inhibition constants were determined for compounds **1**, **2**, and **3**, along with the known inhibitors PAM and PALA as controls. In these experiments, **1** behaved differently than **2** and **3**. **1** was a relatively weak inhibitor (Table 2) and exhibited noncompetitive inhibition with respect to both Asp and CP, **2** and **3** had K_i values approximately 10-fold lower than **1**, and both exhibited competitive kinetics with respect to both Asp and CP. The K_i values for the inhibition of the catalytic subunit with respect to CP by **1**, **2**, and **3** were 2160, 420, and 250 μM, respectively, compared to 5820 μM for PAM and 0.033 μM for PALA (Table 2). Both **2** and **3** showed lower K_i values than **1**, and **3** exhibited a slightly lower K_i value than **2**, in good agreement with our design rationale.

*X-ray Structures of Aspartate Transcarbamoylase in the Presence of **1**, **2**, and **3***. To better understand the mode of binding and any structural changes caused by the inhibitors, X-ray crystallography was employed. Crystals of the enzyme in the presence of **1**, **2**, and **3** diffracted to a maximal resolution of 2.0, 2.0, and 2.5 Å, respectively, in the *P*321 space group. The unit cell dimensions $a = b = 120.59$ and $c = 141.71$ for **1**, $a = b = 119.94$ and $c = 141.97$ for **2**, and $a = b = 120.90$ and $c = 141.61$ for **3** (Table 1) are very similar to those observed for the crystals of the enzyme in the absence of CP (T_{apo}, $a = b = 120.29$ and $c = 142.55$; pdb code 1ZA1). Details of the data collection and refinement of these three structures can be found in Table 1.

The similarity in unit cell dimensions between T_1, T_2, T_3, and T_{apo} structures suggests that the T_1, T_2, and T_3 structures were in the same quaternary structure as T_{apo}. To more accurately determine the quaternary conformation of the T_1, T_2, and T_3 structures, the vertical separation between the upper and lower catalytic subunits for each structure was determined (*37*). The vertical separations for the T_1, T_2, and T_3 structures were 45.55, 44.89, and 45.25 Å, respectively. This compares to the vertical separation of the T state derived from the T_{apo}, T_{CP}, and R_{PALA} structures of 45.5, 45.9, and 56.2 Å, respectively. The vertical separation of T_1, T_2, and T_3 structures is evidence that these three structures are globally in the T-quaternary conformation. Although the binding of PALA to ATCase induces the T to R transition, none of these inhibitors causes the quaternary conformational change. Because these inhibitors were soaked into T-state crystals, it may be argued that crystal packing forces hold the enzyme in the T state; however, when T-state crystals are soaked with PALA, the crystal disintegrates within a few seconds (unpublished observation).

The T_1, T_2, and T_3 structures were compared to the T_{apo} and T_{CP} structures. Overall, the T_1, T_2, and T_3 tertiary structures were closer to the T_{apo} than the T_{CP} structure. For example, the C1 and C6 catalytic chains of the T_1 structure compared to the same chains of the T_{apo} structure and had RMS deviations of 0.259 and 0.304 Å, respectively, whereas when compared to the same chains in the T_{CP} structure, the RMS deviations were 0.987, and 0.915 Å respectively. The trend was the same for T_2 and T_3 structures as well. The 80's loop of both chains in the asymmetric unit in the T_2 and T_3 structures were in a novel conformation unlike that of either the 80's loop conformation in the T_{apo} or the T_{CP} structures with largest differences seen between the T_1 and T_{CP} structures (Figure 3, T_1-A, T_3-A).

Coordination of the Inhibitors in the Active Site of the T_1, T_2, and T_3 Structures. The coordination of the phosphonacetamide group of **1**, **2**, and **3** that most closely matched the position of CP or PAM in the active site was different than the coordination of CP and PAM in the T_{PAM} and T_{CP} structures. The most noteworthy differences were the hydrophobic interactions between Pro266 (not shown) and His134 and the phenyl ring of **2** (Figure 3B, T_2-B) and the absence of backbone interactions to **3** from Leu267, Pro266, and Arg54 (Figure 3, T_3-B).

Table 2: Characterization of Inhibitors[a]

Compound	Structure	Distance (Å)	K_I^{CP} (μM)	K_I^{Asp} (μM)
CP	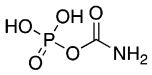	7.3 [b]	---	---
PAM	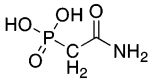	---	5820 (1370)	3870 (560)
PALA	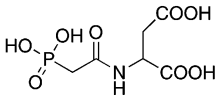	---	0.033 (0.003)	0.021 (0.001)
1	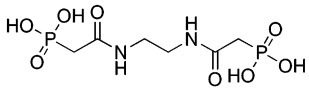	6.0 [c]	2160 (440)	1990 (116)
2	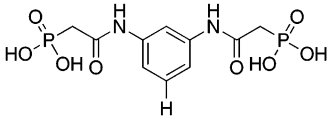	7.0 [c]	420 (32)	420 (11)
3	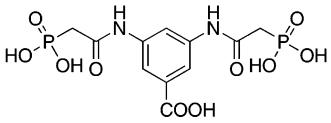	7.0 [c]	250 (20)	310 (8)

[a] K_I^{CP} and K_I^{Asp} values were determined colorimetrically (*41*) at pH 7.0 in 50 mM Hepes buffer at a fixed concentration of 10 mM Asp and 0.4 mM CP, respectively. The numbers in parentheses correspond to error estimates. [b] The distance between the carbonyl carbons of the two CP molecules in the active site of the T_{CP} structure (Figure 1). [c] The distance between the two carbonyl carbons in an extended conformation of the inhibitor.

Noteworthy in all three structures is an interaction between the inhibitor and Thr168, a residue that has not been observed to interact with substrate or substrate analogues in other ATCase structures (Figure 3B). In the T_3 structure, Lys84, from an adjacent catalytic chain, interacts with the carboxylate (Figure 3, T_3-B). In previous structures, Lys84 only interacts with substrates or substrate analogues in the R state. Finally, Arg296, which does not interact with substrates or substrate analogues in structures of the wild-type enzyme in the T state, interacts with **3** (Figure 3, T_3-B).

In addition to a more open conformation of the T-state active sites, there are some positional changes in active site residues compared to those in T_{PAM} and T_{CP}. The largest backbone differences in the active site besides Lys84 in the T_3 structure are residues in the 50's region from Glu50 to Thr55. In the T_{CP} and T_{PAM} structures, Thr53 forms a backbone interaction with the substrate or substrate analogue; however, this interaction is not observed in any of the inhibitor structures reported here (Figure 3B).

***3** Binds More Tightly to the Enzyme than **1** or **2**.* The presence of the hydrophobic phenyl connector ring between the two phosphonacetamide moieties of **2** and **3** hold the phosphate groups in a more rigid conformation, thus enhancing coordination in the ASP domain. For example, in the T_3 structure, **3** is coordinated by five interactions involving Arg229 with Thr168 at hydrogen bonding distances less than 2.75 Å, significantly tighter interactions in the ASP domain than that for structures **1** and **2**. The addition of the carboxylic acid also contributes to the binding of **3** by a specific interaction with Lys84 from the adjacent chain (Figure 3, T_3-B). Figure 3C shows the two CP molecules in the active site of the T_{CP} structure overlaid onto inhibitors **1**, **2**, and **3**. This figure presents the differences in orientation of the phosphonactemide moieties of the three inhibitors compared to the two CP molecules in the active site.

Additionally, significant side chain positional differences are seen in the CP and ASP domain when inspecting T_1, T_2, or T_3 active sites with T_{CP} overlaid, with the largest differences in the T_{CP} and T_3 overlay, most likely induced by the enhanced binding of the phosphonacetamide moiety of **3** (Figure 4).

*Determination of the Quaternary Structure of the Enzyme in the Presence of **1**, **2**, and **3**.* Using a pyrene-labeled version of ATCase, it is possible to use fluorescence spectroscopy to determine if substrates or inhibitors are able to convert ATCase from the T to the R state (*31*). This is made possible by the selective attachment of pyrene at position 241 in the catalytic chain. In the T state, the pyrene labels in the C1 and C4 catalytic chains are far apart, whereas in the R state, after the allosteric transition, they are close together. When two pyrenes are within ~5−10 Å of each other, they show excimer emission (*38*). Thus, in the T state, there is no excimer emission, whereas in the R state, there is substantial excimer emission with a corresponding decrease in monomer emission. Shown in Figure 5A are the emission spectra of ATCase in absence (T-state) and presence of PALA (R-state). Upon adding PALA, the excimer peak at 490 nm increases dramatically, whereas the monomer peak (~400 nm)

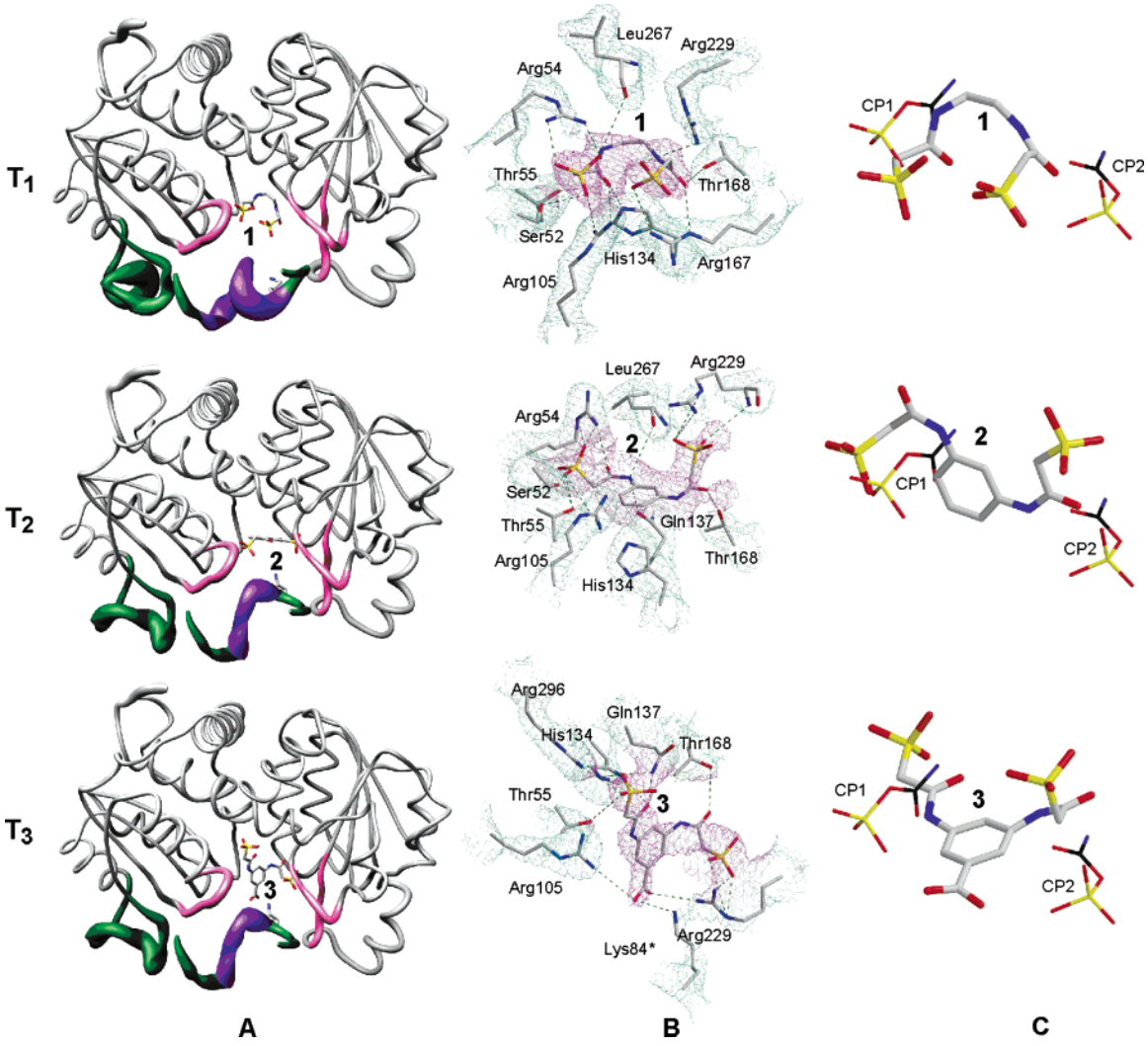

FIGURE 3: Structures of ATCase with **1** (T_1), **2** (T_2), and **3** (T_3) bound. (A) Representation of two adjacent catalytic chains (C1 and C2) of ATCase that comprise one active site. A cartoon representing the change between the T_{CP} structure and the structure with the corresponding inhibitor bound is shown. The width of the tube is proportional to the RMS deviation of the α-carbon atom positions. Also shown is the 80's loop from the adjacent catalytic chain that contributes residues to the active site (80's Loop*) colored in green with the largest differences in the loop colored in magenta. Other regions of notable difference in the α-carbon atom positions of the C1 catalytic chain are residues 50−58, 229−233, and 266−271 (pink). This Figure was drawn with CHIMERA (*43*). (B) Close-up of the active sites of the T_1, T_3, and T_2 structures showing the $2F_o-F_c$ electron density maps contoured at 1.8 σ (blue). Also shown are simulated annealing $2F_o-F_c$ electron density maps contoured at 1.2 σ, with **1**, **2**, and **3** omitted from the map calculation (magenta). Overlaid onto the electron density maps are the refined positions of the residues. (C) Overlay of the T_{CP} active site (*10*) showing the two CP molecules (CP1 and CP2) and the T_1, T_2, and T_3 active sites showing inhibitors **1**, **2**, and **3**. This Figure was drawn with POVScript+ (*42*).

decreases. However, the addition of **1**, **2**, or **3** did not cause any increase in excimer fluorescence at 490 nm, indicating that these inhibitors cannot convert the enzyme to the R-state.

DISCUSSION

Figure 6A shows the T_{apo} active site of ATCase with two molecules of CP bound. Our goal in this project was to design, synthesize, and characterize both functionally and structurally a series of compounds that would completely fill the more open T-state active site of ATCase than the closed R-state active site and, thus, potentially lock the enzyme in the low-activity low-affinity T state. When **1**, **2**, and **3** bind to ATCase, the enzyme remains in the quaternary T structure as determined by both fluorescence measurements with the pyrene-labeled enzyme in solution (Figure 5), and by X-ray crystallography of the enzyme−inhibitor complexes.

The three inhibitors designed as **1**, **2**, and **3**, each bind in the T-state active site and fill the active site pocket. For example, Figure 6B shows **3** bound in the active site on the basis of the T_3 structure. The change of aliphatic functionality connecting the phosphonacetamide groups in **1** to the phenyl moieties in **2** and **3** (Table 2) enhances binding by promoting hydrophobic interactions with Pro266, Leu267, and Pro268. This enhanced binding and specificity was reflected in the significantly lower K_i values of **2** and **3** compared to that of **1**. In addition, the lower K_i value of **3** over **2** can be attributed to the additional carboxylate functionality, which promotes the coordination of **3** with Lys84 from an adjacent catalytic chain (Figures 4 and 6B). The T_3 structure also represents the first instance in which Lys84 from an adjacent chain has been observed to coordinate a substrate or a substrate analogue in a T-state structure.

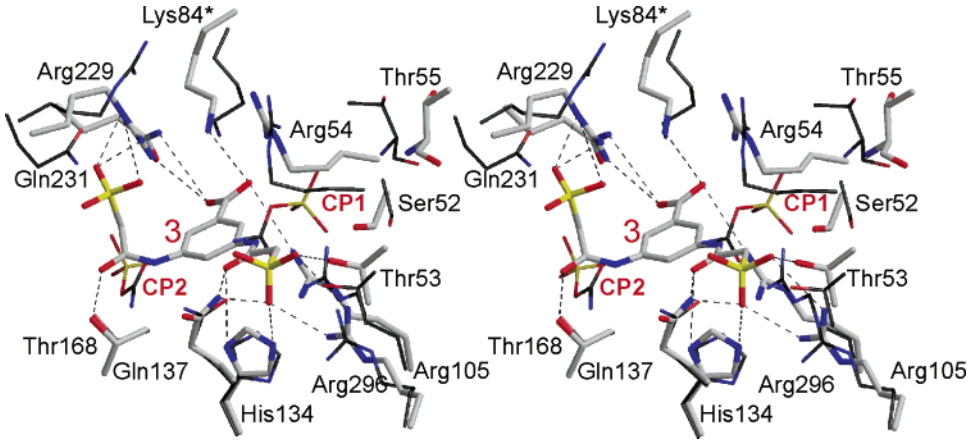

FIGURE 4: Stereoview of the active site of ATCase. Overlay of the T_{CP} (thin, black) onto T_3 (thick, gray). This Figure was drawn with POVScript+ (*42*).

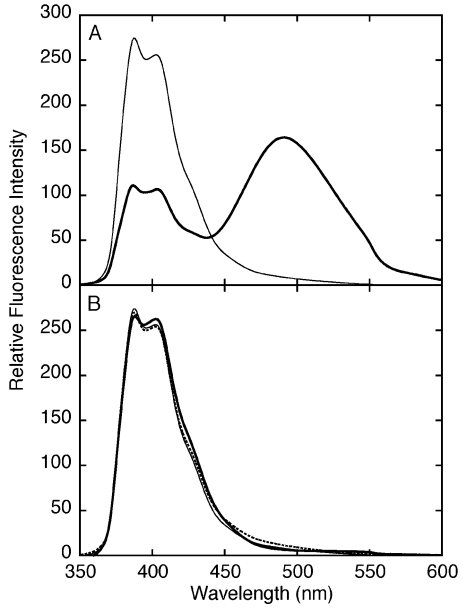

FIGURE 5: Fluorescence emission spectra of the pyrene-labeled ATCase. (A) ATCase (1 μM) in the absence (thin line) and in the presence of 1 μM PALA (heavy line). (B) ATCase in the presence of 1000 μM **1** (dotted line), 660 μM **2** (thin line), and 600 μM **3** (heavy line).

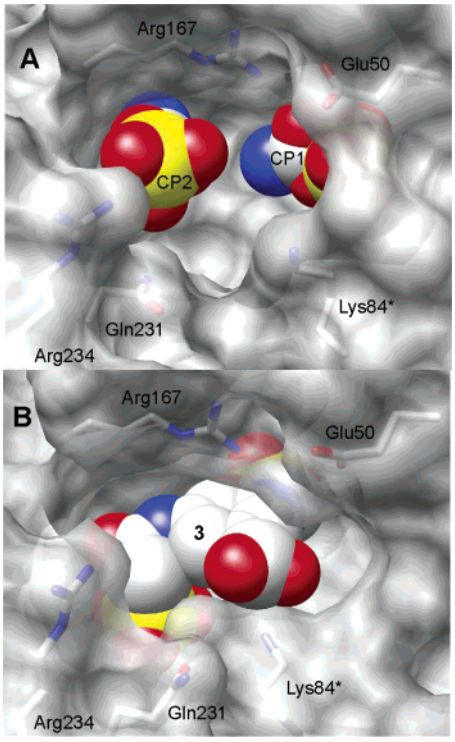

FIGURE 6: (A) Close-up of the active site of the T_{CP} structure (C1 and C2 catalytic chains) (*10*) showing the position of the two CP molecules in a space-filling representation. (B) Close-up of the active site of the T_3 structure (C1 and C2 catalytic chains) showing the position of compound **3** molecules in a space-filling representation. The T_{CP} and T_3 structures were overlaid prior to calculating the surfaces. This Figure was drawn with CHIMERA (*43*).

Although **2** and **3** are reasonably good inhibitors of ATCase, neither one approaches the potency of PALA. This apparent inconsistency is due to the difference in the mode by which these inhibitors bind. When CP binds, it induces conformational changes that enhance its binding, which is an induced fit. This alteration in protein structure can be observed by comparing the T_{apo} and T_{CP} structures (*10*). An induced fit also occurs when PAM binds, but the extent of the conformational change is significantly smaller than that when CP binds (*39*). The extent of the induced fit is even more extreme for PALA because PALA binding results in the closure of the two domains of the catalytic chain, which occurs in conjunction with the T- to R-quaternary conformational change (*8*). PALA binds in a tight complex to the R-quaternary of the enzyme, whereas the weak binding of PAM and CP alone is to the T-quaternary structure. The tertiary and quaternary conformations of the T_1, T_2, and T_3 structures are actually closer to the T_{apo} structure than the T_{CP} structure, suggesting that the binding of these inhibitors, even though they contain a phosphonacetamide functionality, cannot produce the same conformational change induced by the binding of the natural substrate CP or the substrate analogue PAM. Whereas the binding of CP weakens interactions that are required for the stabilization of the enzyme in the T-state, with side chains of the active site approaching their R-state conformation, inhibitors **1**, **2**, and **3** never access the high-affinity R-state active site. A consequence of the

binding of these inhibitors to the T state is to cause the 80's loop to adapt an alternate conformation not observed with the natural substrates. When these inhibitors fill the T-state active site, they do prevent the quaternary conformational change to the R state.

Active Sites of the T_1, T_2, and T_3 Structures Suggest a Mechanism for the Inhibition of Domain Closure. An inspection of active sites of the T_1, T_2, and T_3 structures indicates that there are significant differences in how the phosphonacetamide moiety binds compared to how this moiety binds in the T_{PAM} and R_{PM} structures (*39*). In the T_3 structure, these differences are most pronounced and include an omission of key interactions between **3** and the backbone carbonyls of Pro266 and Leu267 (Figure 3, T_3-B), a new interaction between Arg296 and the phosphate oxygens of **3**, and an interaction with Lys84 from an adjacent catalytic chain with the phenyl carboxylate of **3** (Figure 3, T_3-B).

Arg296 has not been observed to interact with substrates or substrate analogues; however, it has been observed to interact with PAM in the R_{236_PAM} structure (*40*). Arg296 is held in position by hydrogen-bonding interactions with Thr55 and Ser58 of the 50's loop and Thr136, a residue on the cusp of the CP/Asp domains. Arg296 may function in a number of roles, including (i) an initial interaction with carbamoyl phosphate in the active site before the induced fit, (ii) stabilizing the position of the 50's loop, and (iii) helping correctly position CP for the nucleophilic attack by the α-amino group of aspartate (*40*). The role of Arg296 may be more important for the function of ATCase than previously thought because a sequence alignment of a number of transcarbamoylase genes indicated that this residue is conserved. The exact functional role of Arg296 must await direct verification by site-specific mutagenesis. In the T_3 structure, Arg296 is coordinating one of the phosphate oxygens of **3** (Figure 3, T_3-B) instead of the carbonyl oxygen of PAM as seen in the R_{236_PAM} structure. This interaction may prevent the binding of the phosphoacetamide moiety of **3** in the proper orientation to induce the conformational changes that are observed when PAM binds (*39*).

As observed in the T_{CP} structure, critical for the preparation of the high affinity Asp binding site is the movement of the adjacent catalytic chain 80's loop toward the active site pocket to create the necessary electropositive environment for Asp binding (*10*). The novel conformation of the 80's loop seen in the T_1, T_2, and T_3 structures does not create the necessary electropositive environment for Asp binding. These data indicate that inhibitors **1**, **2**, and **3** have the effect of keeping the architecture of the active site in the open conformation rather than promoting the induced fit observed with the natural substrates.

This new class of ATCase inhibitors function by binding to the T-structure and inhibiting the enzyme by filling the T-structure active site. However, as opposed to the binding of CP or PALA, these inhibitors are unable to initiate the conformational change that reorients the active site residues for high-affinity binding. Furthermore, without the induced fit that normally occurs upon the binding of CP, the electrostatic environment of the active site is different than that observed with the natural substrates (or substrate analogues such as PALA). Although **2** and **3** are reasonably good inhibitors of ATCase, these data suggest how the structure of these molecules could be modified to produce even more potent inhibitors. Using structural studies of these second generation inhibitors, it should be possible to develop even more potent inhibitors of ATCase.

REFERENCES

1. Hsuanyu, Y., and Wedler, F. C. (1987) Kinetic mechanism of native *Escherichia coli* aspartate transcarbamylase, *Arch. Biochem. Biophys. 259*, 316−330.
2. England, P., Leconte, C., Tauc, P., and Hervé, G. (1994) Apparent cooperativity for carbamoylphosphate in *Escherichia coli* aspartate transcarbamoylase only reflects cooperativity for aspartate, *Eur. J. Biochem. 222*, 775−780.
3. Gerhart, J. C., and Schachman, H. K. (1968) Allosteric interactions in aspartate transcarbamylase II. Evidence for different conformational states of the protein in the presence and absence of specific ligands, *Biochemistry 7*, 538−552.
4. Wild, J. R., Loughrey-Chen, S. J., and Corder, T. S. (1989) In the presence of CTP, UTP becomes an allosteric inhibitor of aspartate transcarbamylase, *Proc. Natl. Acad. Sci. U.S.A. 86*, 46−50.
5. Lee, L., Kelly, R. E., Pastra-Landis, S. C., and Evans, D. R. (1985) Oligomeric structure of the multifunctional protein CAD that initiates pyrimidine biosynthesis in mammalian cells, *Proc. Natl. Acad. Sci. U.S.A. 82*, 6802−6806.
6. Scully, J. L., and Evans, D. R. (1991) Comparative modeling of mammalian aspartate transcarbamylase, *Proteins 9*, 191−206.
7. Gouaux, J. E., Stevens, R. C., and Lipscomb, W. N. (1990) Crystal structures of aspartate carbamoyltransferase ligated with phosphonoacetamide, malonate and CTP or ATP at 2.8 Å resolution and neutral pH, *Biochemistry 29*, 7702−7715.
8. Jin, L., Stec, B., Lipscomb, W. N., and Kantrowitz, E. R. (1999) Insights into the mechanism of catalysis and heterotropic regulation of *E. coli* aspartate transcarbamoylase based upon a structure of enzyme complexed with the bisubstrate analog N-phosphonacetyl-L-aspartate at 2.1 Å, *Proteins: Struct., Funct., Genet. 37*, 729−742.
9. Stevens, R. C., Gouaux, J. E., and Lipscomb, W. N. (1990) Structural consequences of effector binding to the T state of aspartate carbamoyltransferase: Crystal structures of the unligated and ATP- and CTP-complexed enzymes at 2.6 Å resolution, *Biochemistry 29*, 7691−7701.
10. Wang, J., Stieglitz, K. A., Cardia, J. P., and Kantrowitz, E. R. (2005) Structural basis for ordered substrate binding and cooperativity in aspartate transcarbamoylase, *Proc. Natl. Acad. Sci. U.S.A. 102*, 8881−8886.
11. Collins, K. D., and Stark, G. R. (1971) Aspartate transcarbamylase: Interaction with the transition state analogue N-(phosphonacetyl)-L-aspartate, *J. Biol. Chem. 246*, 6599−6605.
12. Ke, H.-M., Lipscomb, W. N., Cho, Y., and Honzatko, R. B. (1988) Complex of N-phosphonacetyl-L-aspartate with aspartate carbamoyltransferase: X-ray refinement, analysis of conformational changes and catalytic and allosteric mechanisms, *J. Mol. Biol. 204*, 725−747.
13. Kantrowitz, E. R., and Lipscomb, W. N. (1990) *Escherichia coli* aspartate transcarbamoylase: The molecular basis for a concerted allosteric transition, *Trends Biochem. Sci. 15*, 53−59.
14. Swyryd, E. A., Seaver, S. S., and Stark, G. R. (1974) N-(phosphonacetyl)-L-aspartate, a potent transition state analog of aspartate transcarbamylase, blocks proliferation of mammalian cells in culture, *J. Biol. Chem. 249*, 6945−6950.
15. Leyva, A., Appel, H., Smith, P., Lankelma, J., and Pinedo, H. M. (1981) Inhibition of cell growth by N-(phosphonacetyl)-L-aspartate in human and murine cells in vitro, *Cancer Lett. (Shannon, Irel.) 12*, 169−173.
16. Tsuboi, K. K., Edmunds, H. N., and Linda, K. (1977) Selective inhibition of pyrimidine biosynthesis and effect on proliferative growth of colonic cancer cells, *Cancer Res. 37*, 3080−3087.
17. Gouaux, J. E., and Lipscomb, W. N. (1988) Three-dimensional structure of carbamyl phosphate and succinate bound to aspartate carbamyltransferase, *Proc. Natl. Acad. Sci. U.S.A. 85*, 4205−4208.
18. Gerhart, J. C., and Pardee, A. B. (1962) Enzymology of control by feedback inhibition, *J. Biol. Chem. 237*, 891−896.
19. Nowlan, S. F., and Kantrowitz, E. R. (1985) Superproduction and rapid purification of *E. coli* aspartate transcarbamoylase and its catalytic subunit under extreme derepression of the pyrimidine pathway, *J. Biol. Chem. 260*, 14712−14716.

20. Baker, D. P., and Kantrowitz, E. R. (1993) The conserved residues glutamate-37, aspartate-100 and arginine-269 are important for the structural stabilization of *Escherichia coli* aspartate transcarbamoylase, *Biochemistry 32*, 10150−10158.
21. Gerhart, J. C., and Holoubek, H. (1967) The purification of aspartate transcarbamylase of *Escherichia* coli and separation of its protein subunits, *J. Biol. Chem. 242*, 2886−2892.
22. Laemmli, U. K. (1970) Cleavage of structural proteins during the assembly of the head of bacteriophage T4, *Nature 227*, 680−685.
23. Davis, B. J. (1964) Disc electrophoresis-II method and application to human serum proteins, *Ann. N.Y. Acad. Sci. 121*, 680−685.
24. Ornstein, L. (1964) Disc electrophoresis. I. Background and theory, *Ann. N.Y. Acad. Sci. 121*, 321−349.
25. Kim, K. H., Pan, Z., Honzatko, R. B., Ke, H.-M., and Lipscomb, W. N. (1987) Structural asymmetry in the CTP-liganded form of aspartate carbamoyltransferase from *Escherichia coli*, *J. Mol. Biol. 196*, 853−875.
26. Pflugrath, J. W. (1999) The finer things in X-ray diffraction data collection, *Acta Crystallogr., Sect. D 55*, 1718−1725.
27. Brunger, A. T., Adams, P. D., Clore, G. M., DeLano, W. L., Gros, P., Grosse-Kunstleve, R. W., Jiang, J.-S., Kuszewski, J., Nilges, N., Pannu, N. S., Read, R. J., Rice, L. M., Simonson, T., and Warren, G. L. (1998) Crystallography and NMR system (CNS): A new software system for macromolecular structure determination, *Acta Crystallogr., Sect. D 54*, 905−921.
28. McRee, D. E. (1999) XtalView/Xfit: A versatile program for manipulating atomic coordinates and electron density, *J. Struct. Biol. 125*, 156−165.
29. Laskowski, R. A., MacArthur, M. W., Moss, D. S., and Thornton, J. M. (1993) PROCHECK: A program to check the stereochemical quality of protein structures, *J. Appl. Crystallogr. 26*, 283−291.
30. Goodsell, D. S., Morris, G. M., and Olson, A. J. (1996) Automated docking of flexible ligands: applications of AutoDock, *J. Mol. Recognit. 9*, 1−5.
31. West, J. M., Tsuruta, H., and Kantrowitz, E. R. (2004) A fluorescent probe-labeled aspartate transcarbamoylase that monitors the allosteric conformational state, *J. Biol. Chem. 279*, 945−951.
32. Gu, Y. G., Zhang, X., Clark, R. F., Djuric, S. W., and Ma, Z. (2004) The stereoselective synthesis of novel macrolide antibacterial agents via an intramolecular 1,3-dipolar cycloaddition of azomethine ylide, *Tetrahedron Lett. 45*, 3051−3053.
33. Lee, H. B. (1988) Perfluoro and chloro amide derivatives of aniline and chloroanilines. A comparison of their formation and gas chromatographic determination by mass selective and electron capture detectors, *J. Chromatogr. 457*, 267−78.
34. Reddy, P. S. N., and Nagaraju, C. (1991) A new synthesis of 2-aryl-2H-pyrazino[2,1-b]quinazoline-3,6(1H,4H)-diones, *Synth. Commun. 21*, 173−81.
35. Heinicke, J., Gupta, N., Surana, A., Peulecke, N., Witt, B., Steinhauser, K., Bansal, R. K., and Jones, P. G. (2001) Synthesis of 1H-1,3-benzazaphospholes: substituent influence and mechanistical aspects, *Tetrahedron 57*, 9963−9972.
36. Kurz, T., and Widyan, K. (2004) A convenient synthesis of 3-amino-4-imino(thioxo)-imidazolidin-2-ones, *Tetrahedron Lett. 45*, 7049−7051.
37. Stieglitz, K., Stec, B., Baker, D. P., and Kantrowitz, E. R. (2004) Monitoring the transition from the T to the R state in *E. coli* aspartate transcarbamoylase by X-ray crystallography: Crystal structures of the E50A mutant in four distinct allosteric states, *J. Mol. Biol. 341*, 853−868.
38. Birks, J. B. (1970) *Photophysics of Aromatic Molecules*, Wiley-Interscience, London.
39. Gouaux, J. E., and Lipscomb, W. N. (1990) Crystal structures of phosphonoacetamide ligated T and phosphonoacetamide and malonate ligated R states of aspartate carbamoyltransferase at 2.8 Å resolution and neutral pH, *Biochemistry 29*, 389−402.
40. Stieglitz, K. A., Dusinberre, K. J., Cardia, J. P., Tsuruta, H., and Kantrowitz, E. R. (2005) Structure of the *E.coli* aspartate transcarbamoylase trapped in the middle of the catalytic cycle, *J. Mol. Biol. 352*, 478−486.
41. Pastra-Landis, S. C., Foote, J., and Kantrowitz, E. R. (1981) An improved colorimetric assay for aspartate and ornithine transcarbamylases, *Anal. Biochem. 118*, 358−363.
42. Fenn, T. D., Ringe, D., and Petsko, G. A. (2003) POVScript+: A program for model and data visualization using persistence of vision ray-tracing, *J. Appl. Crystallogr. 36*, 944−947.
43. Pettersen, E. F., Goddard, T. D., Huang, C. C., Couch, G. S., Greenblatt, D. M., Meng, E. C., and Ferrin, T. E. (2004) UCSF Chimera—a visualization system for exploratory research and analysis, *J. Comput. Chem. 25*, 1605−1612.

BI0601095